博士論文

Coordination between olfactory cortex sharp-wave activity and orbitofrontal cortex slow-wave activity during slow-wave sleep

（徐波睡眠時における嗅皮質鋭波と前頭眼窩皮質徐波との協調的活動）

鬼沢　菜穂美

Table of Contents

Abstract

During slow-wave sleep, inter-areal communications via coordinated slow oscillatory activities occur in the large-scale networks of the mammalian neocortex. Because olfactory cortex (OC) areas, which belong to paleocortex, show characteristic sharp-wave activity during slow-wave sleep, I examined whether OC sharp-waves in freely behaving rats occur in temporal coordination with up- and down-states of the orbitofrontal cortex (OFC) slow oscillation. Simultaneous recordings of local field potentials and spike activities in the OC and OFC showed that during the down-state in the OFC, the OC also exhibited down-state with greatly reduced neuronal activity and suppression of sharp-wave generation. OC sharp-waves occurred during two distinct phases of the up-state of the OFC: early phase sharp-waves occurred at the start of up-state shortly after the down-to-up transition in the OFC, while late phase sharp-waves were generated at the end of up-state shortly before the up-to-down transition. Such temporal coordination between neocortical up- and down-states and olfactory system sharp-waves was observed between the prefrontal cortex areas (orbitofrontal cortex and medial prefrontal cortex) and the OC areas (anterior piriform cortex and posterior piriform cortex). These results suggest that during slow-wave sleep, OC and OFC areas communicate preferentially in specific time windows shortly after

the down-to-up transition and shortly before the up-to-down transition.

Introduction

Slow-wave sleep provides a specific time window for off-line communication among wide areas of the mammalian cerebral neocortex and subcortical structures in the forebrain without disturbance by sensory inputs from the external world (Contreras and Steriade 1995; Steriade and Contreras 1995; Steriade et al. 2001; Timofeev et al. 2001). During slow-wave sleep, the neocortex is isolated from external sensory inputs and shows intrinsically-generated coordinated population activity with large-amplitude slow oscillations of local field potentials (Steriade et al. 1990; Steriade et al. 1993c). This slow oscillatory activity propagates occasionally across whole areas of the neocortex, suggesting the coordination of activity across large-scale cortical networks (Massimini et al. 2004; Murphy et al. 2009; Vyazovskiy et al. 2011).

The neocortex slow oscillations consist of an up-state of enhanced neuronal activity and inter-areal communication and down-state of neuronal silence (Mölle and Born 2011; Steriade et al. 1993c). The up-state is characterized by depolarized membrane potential levels of neocortical neurons and is associated with depth-negative, surface-positive local field potentials. During the down-state, in contrast, neocortex neurons are hyperpolarized and each neocortex area shows depth-positive, surface-negative local field potentials (Contreras and Steriade 1995; Steriade et al.

1993c). Because the neocortical activity associated with the slow oscillations propagates to the hippocampus and thalamus, activities of the hippocampus and thalamus are finely coordinated with the up- and down-states of the neocortex. Only during the neocortical up-state, hippocampus generates sharp-wave/ripple events and thalamus gives rise to spindles (Mölle and Born 2011). Thus, during slow-wave sleep, the up-state of the neocortex provides a temporal framework in which reciprocal communication occurs between the neocortex and hippocampus and between the neocortex and thalamus.

The anterior piriform cortex (APC), a major area of the olfactory cortex (OC), generates characteristic sharp-wave (SPW) activity during slow-wave sleep (Manabe et al. 2011). The APC has direct axonal projections to the orbitofrontal cortex (OFC: lateral orbital cortex and ventrolateral orbital cortex) and agranular insular cortex, while these neocortical areas send top-down axonal projections back to the APC (Illig 2005; Ray and Price 1992). In addition, the APC indirectly interacts with these neocortical areas via the endopiriform nucleus and thalamus. For example, pyramidal cells in the APC activate neurons in the endopiriform nucleus and claustrum which then send signals to the agranular insular cortex and OFC (Fu et al. 2004; Lipowska et al. 2000). Furthermore, neurons in the deep part of the APC project axons to the mediodorsal and submedial nuclei of the thalamus, and these thalamic nuclei have reciprocal projections

with the OFC and agranular insular cortex (Krettek and Price 1977; Neville and Haberly 2004; Ray and Price 1992).

These direct and indirect axonal connections between the APC and OFC raise the possibility that SPW events of the APC are coordinated with the up- or down-states of the OFC during slow-wave sleep. It has been shown in urethane-anesthetized rats that sharp-wave activity of the piriform cortex occurs in synchrony with the slow-wave activity in the mediodorsal nucleus of the thalamus (Courtiol and Wilson 2014). However, it is not understood whether and how interactions between the APC and OFC occur during natural slow-wave sleep.

To address these questions, I recorded local field potentials and spike activities simultaneously in the APC and OFC of freely behaving rats during the whole period of a natural sleep. Here, I demonstrate the presence of clear temporal coordination between the generation of SPWs in the APC and up- and down-states of the OFC. Results from multi-unit recordings of the APC and OFC support the idea of enhanced interaction between the APC and OFC during the OFC up-state and reduced interaction during the down-state. These results suggest that the up-state of the slow oscillations in the OFC provides a common temporal framework for the large-scale interactions among the OFC areas and olfactory cortex areas during slow-wave sleep.

Materials and Methods

Animals

Male Long-Evans rats purchased from Japan SLC were housed individually in plastic cages (345 × 403 × 177 mm) or metallic cages (350 × 400 × 300 mm) at 25 °C under a 12-h light/dark cycle with light on at 5:00 AM. All experiments were conducted in accordance with the guidelines of the Physiological Society of Japan and were approved by the Experimental Animal Research Committee of the University of Tokyo.

Surgery for electrode implantation

Details of the surgical preparation and chronic electrophysiological recording methods used in the present study have been reported previously (Manabe et al. 2011). Adult male Long-Evans rats (294–475 g at the time of surgery) were anesthetized with ketamine (67.5 mg/kg, i.p.) and medetomidine (0.5 mg/kg, i.p.) for surgery to implant stimulation and recording electrodes at appropriate places in the brain.

For olfactory bulb (OB) stimulation, a bipolar electrode was implanted in the OB (8.0 mm anterior to the bregma, 1.3 mm lateral to the midline, 2.5 mm deep from the skull surface). For recordings of single- and multi-unit activities in the APC and OFC, a

multisite microdrive array that allows targeting of two brain regions and independent adjustment of 16 individual tetrodes was implanted in the APC (0.0 mm anterior to the bregma, 4.2 mm lateral to the midline) and OFC (4.0 mm anterior to the bregma, 2.5 mm lateral to the midline). Individual tetrodes consisted of four twisted polyimide-coated tungsten wires (12.5 μm diameter; California Fine Wire). The microdrive array was fixed to the skull with dental acrylic and anchor screws.

To record local field potentials, twisted polyimide-coated tungsten wires (50 μm diameter; California Fine Wire) were implanted into the OB (8.0 mm anterior to the bregma, 1.25 mm lateral to the midline, 2.3 mm deep from the skull surface), APC (2.0 mm anterior to the bregma, 2.8 mm lateral to the midline), PPC (3.1 mm posterior to the bregma, 4.0 mm lateral to the midline), OFC (3.7 mm anterior to the bregma, 2.5 mm lateral to the midline, 4.0 mm from the skull surface) and mPFC (4.2 mm anterior to the bregma, 0.5 mm lateral to the midline, 2.0 mm from the skull surface). The positions of the electrode tips in layer III of the APC and PPC were determined by monitoring the configuration of OB-evoked local field potentials. For neocortical EEG recording, a stainless screw was threaded into the bone above the occipital cortex (6.3 mm posterior to the bregma, 3.0 mm lateral to the midline). Two further screws were threaded into the bone above the cerebellum for reference. For electromyograms (EMGs) recording,

Teflon-insulated stainless-steel electrodes were implanted in the neck muscle. To monitor respiration pattern, a thermocouple (0.23 mm diameter, Teflon coated; World Precision Instruments) was implanted in a nasal cavity through a hole made in the dorsal skull and secured to the scull with dental acrylic.

Electrophysiological recordings in freely behaving animals

Animals were allowed to recover from surgery for at least 1 week before recording. For recordings during sleep, rats were allowed to behave freely in a well-habituated bedded cage. Recording was performed during the light period (5:00 AM to 5:00 PM). The recording electrodes were connected with an electrode interface board (Neuralynx) on the microdrive. Electrical signals were obtained using a Cheetah recording system (Neuralynx). For unit recordings, the signals were sampled at 32 kHz and band-pass filtered at 600–6,000 Hz. For local field potential recordings, the signals were sampled at 16 kHz and band-pass filtered at 0.1–6,000 Hz. Unit recordings were obtained with tetrode depth adjusted on each recording day to acquire activity from new neurons. The positions of the tetrode tips in the layer of the piriform cortex were determined by monitoring the configuration of the local field potential evoked by electrical stimulation of the OB. After the experiments, small lesions were made by current injection for later

histological examination of the recording sites.

Data analysis

I used the Klustakwik (by K.D. Harris) and MClust software (by A.D. Redish) for off-line spike sorting (Harris et al. 2000) and Spike2 software (Cambridge Electronic Design) for analysis.

Behavioral states were determined by the following method that was modified from previous reports (Manabe et al. 2011; Tsuno et al. 2008). I classified four different behavioral states in freely behaving animals: wakefulness state, slow-wave sleep state, light sleep state, and rapid eye movement (REM) sleep state. These states were determined off-line by the combination of neocortical EEG pattern, neck muscle EMG activity and respiration pattern in 10 s epochs. During the transition periods from wakefulness state, light sleep state or REM sleep state to slow-wave sleep state and from slow-wave sleep state to the other three states, the states were determined in 1 s epochs. Wakefulness state was characterized by the presence of the fast neocortical EEG activity and the tonic activity of the neck muscle EMG activity. Sleep states (slow-wave sleep, light sleep and REM sleep) were determined by the presence of the slow-osicillatory EEG activity (except for REM sleep) and the absence of tonic activity

of the neck muscle EMG activity (Tsuno et al. 2008). The three sleep states were determined by the neocortical EEG pattern (Tsuno et al. 2008) and the respiration pattern. Slow-wave sleep state was determined by the high slow-wave (0.5–1.5 Hz) and delta-wave (1.5–4 Hz) power of the neocortical EEG (Manabe et al. 2011) and stable slow respiration. Light sleep state was characterized by the mixture of fast-wave, slow-wave and spindle activities (Tsuno et al. 2008) and stable respiration with amplitude smaller than that of slow-wave sleep. REM sleep was determined by a high-frequency, low-amplitude EEG (Tsuno et al. 2008) and unstable respiration pattern at frequencies faster than that of light sleep state.

APC sharp-waves (APC-SPWs) were characterized as large sharp negative local field potentials with a duration less than 200 msec recorded from the layer III of the APC (Manabe et al. 2011). To qualify APC-SPW potentials, the local field potential was downsampled to 100 Hz and bandpass filtered at 2–20 Hz. Mean and standard deviation (SD) of the local field potential amplitude were calculated. The threshold amplitude for SPW detection was set to 4 SDs above the mean amplitude. Among high-amplitude potentials above the threshold, sharp negative potentials with a duration less than 200 msec were selected and regarded as SPWs.

Tentative down-states in the OFC during slow-wave sleep were characterized as large

positive peaks of local field potentials recorded in the deep layer (layers V/VI) of the OFC (Fig. 2). To quantify the tentative peak of down-state, local field potential in the OFC was down-sampled to 100 Hz and low-pass filtered at 20 Hz. Mean and SD of local field potential amplitude were calculated. The threshold for tentative peak of down-state detection was set to 2 SDs positive to the mean (Fig. 2). Using this tentative peak of down-state, I determined the period of down-state by the following way. First, peri-peak of down-state time histograms of OFC multiunits activities were calculated in 10-ms bin, and mean and SD of the OFC multiunits firing frequency within –500 to +500 msec from the time of the peak of down-state were calculated. Second, two time points that fell to the mean –2 SDs were calculated for each animal for each experiment (n= 8 experiments from 3 rats). Averaged time points that fell to the mean –2 SDs were –81.25 msec and –3.75 msec. Because the bin width in the histogram was 10 msec, I estimated that the down-state period was –90 msec to 0 msec from the peak of down-state.

Recordings were performed for 1–3 h during the light period (5:00 AM to 5:00 PM). The whole period of natural sleep that occurred during the recording period was used for analysis. The average duration of sleep was 2,677 sec per rat. Mean numbers of events were 1,902 OFC down-state events, 1,850 mPFC down-state events, 1,939

APC-SPW events, 2,222 PPC-SPW events, and 2,370 OB-SPW events per rat. All events were used for analysis.

Peri-down-state time histograms and peri-SPW time histograms were calculated in 10-msec bins. The tendency of spike discharges to become silent with the down-state was considered significant when the firing frequency of at least 3 bins among those within –90 to 0 msec from the peak time of the down-state (down-state period determined by the above method) fell to a mean – 2 SDs of background firing frequency (during –500 to –200 msec and during +200 to +500 msec) (Fig. 1, B and E). The tendency of spike discharges to synchronize with SPW events was considered significant when the firing frequency of at least one bin among those within –100 to +100 msec from the time of the trough of SPW exceeded a mean + 3 SDs of background firing frequency (during –300 to –200 msec and +200 to +300 msec) (Fig. 6).

To determine the frequency of APC-SPW events during the up-state and that during the down-state of the OFC, the number of APC-SPW events during up-state was divided by the total time of up-state while the number of them during down-state was divided by the total time of down-state. As described above, down-state period was estimated by the time window from –90 to 0 msec before the peak time of the down-state. I counted

APC-SPW events that occurred within the down-state periods. I then counted APC-SPW events that occurred outside the down-state periods and considered them as APC-SPWs during the up-state. The total time of down-state was calculated as 90 msec × number of down-state events. The total time of up-state was obtained by subtracting the total down-state time from the total time of slow-wave sleep. I then compared the frequency of APC-SPW events between the up-state and down-state periods. Differences in the frequency of APC-SPW generation between the up-state and down-state were statistically analyzed using paired t-test (significance level, $p < 0.05$) (Fig. 3C).

An OFC down-state that occurred in synchrony with an APC down-state (less than 50 msec difference in peak time of OFC and APC down-states) was defined as a global OFC down-state. A local OFC down-state was defined when the OFC down-state did not accompany an APC down-state (within 50 msec). To compare the spike activity pattern of OFC and APC neurons among up-state, global down-state and local down-state, I calculated spike frequency of these neurons during the three periods. Statistical analysis of significant differences was performed using one-way ANOVA with post hoc Tukey test (significance level, $p < 0.05$) (Fig. 5C). To compare the frequency of APC-SPW occurrence shortly before and after the global down-state and

that shortly before and after the local down-state, the averaged frequency of APC-SPW occurrence during –200 to +200 msec from the peak time of down-states was calculated. The group difference in the frequency of APC-SPW occurrence was verified by the paired t-test (significance level, $p < 0.05$) (Fig. 5E).

To calculate the peri-OFC down-state time histogram for Fig. 8C, the number of mPFC down-state events in each bin was divided by the total number of mPFC down-state events within –250 to +250 msec from the peak time of the OFC down-state. The probability of mPFC down-state events in each bin was then calculated for each animal. The averaged probability of mPFC down-state events in each bin was then calculated using all the data from different experiments and from different animals.

To obtain phase histograms of APC-SPW, PPC-SPW and OB-SPW events during up-state, one cycle of up-state in the OFC and mPFC (i.e. from the start of up-state to the end of up-state) was divided into 360° (one cycle = 30 bins). Because the down-state period was defined to start at –90 msec before the peak of down-state and end at the down-state peak in this study, the peak of down-state (i.e., the end of down-state) was set as the start of up-state. The time point at –90 msec before the peak of subsequent down-state (i.e., the start of the subsequent down-state) was set to the end of up-state. The number of SPW events in each bin was divided by the total number of SPW events

in one cycle. The probability of SPW events in each bin was then calculated for each animal. The averaged probability of SPW events in each bin for all the data from different experiments and from different animals was then calculated. Analysis was done for the up-state cycles that had duration from 0.25 to 2.0 sec (Fig. 4C, 8B).

Histology

After the experiments, the animals were deeply anesthetized with urethane and perfused first with PBS followed by 4% paraformaldehyde (PFA) in phosphate buffer (PB), pH 7.4. Brains were postfixed in 4% PFA in PB at 4°C. Coronal sections of the brain (40-μm thick for brains with unit recordings, 50-μm thick for brains with local field potential recordings) were cut on a vibratome, mounted on glass slides, and stained with cresyl violet.

Results

Synchronization of slow oscillations between OFC and APC

To examine the possibility that the OFC interacts with the APC at specific time windows during slow-wave sleep, I recorded local field potentials and multi-unit spike activities simultaneously in the deep layer (layers V and VI) of the OFC and the deep layer (layer III) of the APC of freely behaving rats. During slow-wave sleep periods, the local field potential in the OFC showed slow-wave activity (0.5–4 Hz), with each oscillatory cycle consisting of a large slow positive potential followed by a longer slow negative potential (Fig. 1A, OFC-LFP). Multi-unit spike activities in the OFC indicated that OFC neurons showed enhanced spike activities during the slow negative potential, indicating that the occurrence of the slow negative potential corresponds in time with the up-state of the OFC (Fig. 1, A and B) (Contreras and Steriade 1995; Steriade et al. 1993c). In striking contrast, the slow positive potential was associated with silencing of the spike activities of OFC neurons (Fig. 1, A and B). This shows that the slow positive potential corresponds in time with the down-state of the OFC.

To roughly estimate the time window of the OFC down-state based on the configuration of the slow oscillatory potentials, I first assumed four different levels of

tentative threshold potential that differentiate the depth-negative potential (up-state) and depth-positive potential (down-state) (Fig. 2A). By comparing the timing of the down-state defined by this method and that of the diminished spike activities of OFC neurons, I found that the down-state determined by the threshold of mean + 2 SDs provided the best fit with the temporal framework of the down-state determined by the diminished spike discharges (Fig. 2, A and B). Accordingly, I set the threshold to detect the peak of down-state as a mean + 2 SDs of the filtered OFC local field potential in this study. Fig. 2C shows examples of the spike activities of individual OFC neurons during the down-state detected by the above method. Although it was clear from the definition of down-state period, a majority of the OFC neurons (73%, 133/183 cells) showed a significant silence (see Method) during the down-state (Fig. 1B).

Local field potentials in the APC also showed slow-wave activity during slow-wave sleep (Fig. 1A). Although the APC shows slow oscillatory potentials in phase with the respiration cycle during wakefulness (Mori et al. 2013), the slow-wave activity during slow-wave sleep occurred relatively independently of the respiration cycle (Fig. 1A). Each cycle of APC slow-wave activity consists of a slow depth-positive potential and a slow depth-negative potential.

Simultaneous recordings of local field potentials in the OFC and APC indicated that

slow depth-positive and depth-negative potentials in the APC tended to synchronize with those in the OFC. Local field potentials in the APC showed high coherence with those of the OFC in the range between 1 and 4 Hz (Fig. 1, C and D). These results suggest that slow-wave activity in the APC tends to occur in synchrony with slow-wave activity in the OFC during slow-wave sleep. In accordance with this idea, the majority of APC neurons showed reduced spike activities during the OFC down-state, and about one-fifth of APC neurons (22%, 27/121 cells) showed a significant silence (see Method) during the down-state (Fig. 1E).

It should be noted that the down-state in the OFC did not always accompany the down-state in the APC and that some APC neurons were occasionally active during the OFC down-state (Fig. 1A). In other words, down-states in the OFC can be classified into two types: OFC down-states with an accompanying APC down-state (global OFC down state) and OFC down-states without an accompanying APC down-state (local OFC down-state), as will be described in detail later.

Synchronization between APC-SPW events and the OFC up- and down-states

APC shows characteristic sharp-waves (SPWs) that were superimposed on slow negative potentials (APC up-state) during slow-wave sleep (arrows in Fig. 1A) and that

each SPW was associated with highly-synchronized spike discharges of APC neurons (Manabe et al. 2011). Given that numerous APC neurons show synchronized spike discharges during APC-SPW events (Manabe et al. 2011) and that APC-SPWs occurred mainly during the slow negative potential in the APC (Fig. 1A), I further examined the temporal relationship between SPW events in the APC and slow-wave activity in the OFC during slow-wave sleep. As shown in Figs. 3, A, B, and C, the occurrence of SPW events in the APC was greatly reduced during the down-state of the OFC. A majority of APC-SPW events temporally coincided with the up-state of the OFC.

To more closely examine the timing of APC-SPW occurrence in relation to the time course of the OFC up-state, a convenience sample of 15 traces of OFC slow-wave cycles with various durations were arbitrarily selected and aligned in reference to the start of up-state (Fig. 4A). The start of up-state was defined as the time point corresponding to the end of the preceding OFC down-state (the time point of the peak of the preceding down-state). Fig. 4A clearly shows that APC-SPWs (gray vertical bar) tend to occur shortly before and shortly after the OFC down-state.

To examine the timing of occurrence for all the recorded APC-SPW events, I tentatively divided one cycle of OFC up-state into 360° (from the peak of a down-state (0°) to the time point at –90 msec before the peak of next down state (360°); one bin =

12°) and calculated APC-SPW phase histograms (Fig. 4C). As shown in Fig. 4C, APC-SPWs tended to occur shortly before and shortly after the OFC down-state. I tentatively defined three phases for each OFC up-state: an initial one-third (0°–120°, phase I) that starts from the peak of the preceding down state (0°), a middle one-third (120°–240°, phase II), and a final one-third (240°–360°, phase III) (Fig. 4C). APC-SPW events occurred at all three phases of the OFC up-state. However, statistical analysis of the timing of APC-SPW occurrence indicated that the APC-SPWs tended to occur shortly after the transition from the down-state to the up-state of the OFC (during phase I) and shortly before the transition from the up-state to the down-state in the OFC (during phase III) (Fig. 4C). These results indicate that there are two major types of APC-SPW — early phase APC-SPWs that occur in phase I and late phase APC-SPWs that occur in the phase III — and suggest that enhanced interactions between OFC and APC occur at two distinct phases of up-state; i.e. at the early phase of up-state shortly after the down-to-up transition of the OFC slow-wave activity and at the late phase shortly before the up-to-down transition.

APC-SPWs in association with global and local OFC down-states

As described above, the OFC down-state did not always synchronize with the APC

down-state: while the down-state of the OFC sometimes coincided with the down-state of the APC (global OFC down-state in Fig. 5A), the OFC down-state occasionally occurred when the APC was at the up-state (local OFC down-state in Fig. 5A). Approximately 30% of all OFC down-state events were global down-states while the remaining 70% were local down-states. Although it was clear from the definition of down-state period, OFC neurons were silent during both the global and local down-states (Fig. 5, B and C). On the other hand, APC neurons showed reduced spike activity only during the global OFC down-state, and did not show reduced spike activity during the local OFC down-state (Fig. 5, B and C). I compared the frequency of APC-SPW occurrence shortly before and after the global OFC-APC down-state (Fig. 5D, left) with that shortly before and after the local OFC down-state (Fig. 5D, right), and found that APC-SPWs occurred more frequently in the time windows before and after the global OFC down-state than before and after the local OFC down-state (Fig. 5E). These results suggest that stronger interactions between APC and OFC occur in the time windows shortly before and after the global OFC-APC down-states compared with those shortly before and after the local OFC down-states.

Interaction between the OFC and the APC during the APC-SPW events

Because numerous APC neurons show synchronized spike discharges during APC-SPWs (Manabe et al. 2011), I examined whether individual OFC neurons show spike discharges in synchrony with the APC-SPWs using simultaneous recording of APC-SPWs and single-unit spikes in the OFC. The peri-APC-SPW time histogram of spike discharges of OFC neurons (Fig. 6) indicated that about 45% of recorded neurons in the OFC (82/183 OFC neurons) showed enhanced spike discharges during the APC-SPWs. These observations suggest that enhanced excitatory interactions between APC neurons and OFC neurons occur in synchrony with APC-SPW events shortly after the down-to-up transition and shortly before the up-to-down transition of OFC.

The enhanced excitatory interactions between OFC and APC suggests the following two possibilities of the direction of signal transfer: (1) SPW-related synchronized discharges of APC neurons drive numerous OFC neurons, and (2) synchronized discharges of OFC neurons during the OFC up-state drive the synchronized discharges of APC neurons and generate APC-SPWs. To address the question of the direction of signal transfer, I compared the timing of spike generation between OFC and APC neurons with reference to APC-SPWs.

As exemplified in Fig. 6, the probability of spike discharges of OFC neurons peaked at various phases of the APC-SPW event. About 60% (49/80) of OFC neurons showed a

peak of spike discharge probability in the descending phase (before the trough) of the APC-SPW, while the remaining 40% (33/80) of OFC neurons showed a peak in the ascending phase of the APC-SPWs. As reported previously, the probability of spike discharge for most APC neurons peaks in the middle of the descending phase of APC-SPW events (Manabe et al. 2011). Comparison of the present and these previous results suggests that although the peak of spike discharge probability of APC neurons tends to precede that of OFC neurons during the APC-SPW events, the timing of the discharge of OFC neurons largely overlaps that of APC neurons. These results suggest that signal transfers during APC-SPWs occur in both the APC-to-OFC and OFC-to-APC directions.

Coordination of up- and down-states and SPW events across wide areas of the prefrontal cortex and wide areas of the central olfactory system

As reported previously, APC-SPWs propagate widely to numerous areas of the olfactory cortex (anterior olfactory nucleus, posterior piriform cortex and olfactory tubercle) and olfactory bulb (Manabe et al. 2011; Narikiyo et al. 2014; Komano-Inoue et al. 2014). Furthermore, neocortical slow-wave activity generates synchronized up- and down-states across wide areas of the prefrontal cortex during slow-wave sleep

(Massimini et al. 2004; Murphy et al. 2009; Vyazovskiy et al. 2011). These results suggest that coordination of the up-state in the prefrontal cortex and the SPW events in the olfactory cortex occurs not only between the APC and OFC but also across many areas of both the olfactory cortex and prefrontal cortex. To examine this possibility, I made simultaneous recordings of local field potentials from the deep layers of the orbitofrontal cortex (OFC), medial prefrontal cortex (mPFC), anterior piriform cortex (APC) and posterior piriform cortex (PPC) (Fig. 7). Furthermore, because APC-SPWs propagate to the olfactory bulb (OB), I also recorded local field potentials from the deep layer (granule cell layer) of the OB. As shown in Figs. 7, A, B and C, up-to-down and down-to-up transitions of slow-wave activity tended to synchronize not only between neocortex areas (OFC and mPFC) but also among the neocortex areas and olfactory cortex areas (APC and PPC), albeit that the slow-wave synchronization between the OFC and mPFC was more coherent than that between the OFC and APC. Weak synchronization of slow-wave activity was also noted between the neocortex areas (OFC and mPFC) and OB (Figs.7, A–C). Fig. 8A shows that the occurrence of APC-SPW, PPC-SPW, and OB-SPW events was greatly reduced during both the OFC and mPFC down-states. Furthermore, not only APC-SPWs but also PPC-SPWs and OB-SPWs tended to occur shortly after and shortly before the OFC down-states (Fig.

8B, left column). The same results were observed in the mPFC down-state (Fig. 8B, right column). This is in agreement with the observation that a majority of OFC down-state occurred in synchrony with mPFC down-state (Fig. 8C).

These observations suggest that SPW-mediated interactions of olfactory cortex neurons occur not only with OFC neurons but also with mPFC neurons. Given that APC-SPWs are transmitted to the OB and olfactory tubercle (Manabe et al. 2011; Narikiyo et al. 2014; Komano-Inoue et al. 2014), these observations suggest that signals originating from SPW-mediated interactions between prefrontal areas (OFC and mPFC) and olfactory cortex areas (APC and PPC) may be transmitted to the OB and olfactory tubercle. In other words, SPW-associated synchronized neuronal activity of the large-scale networks of the central olfactory system (APC, PPC, olfactory tubercle and OB) may occur in temporal association with the enhanced neuronal activities of the large-scale networks of the OFC and mPFC during the time windows of shortly after the down-to-up transition and shortly before the up-to-down transition of the prefrontal cortex.

Discussion

Temporal coordination of olfactory cortex SPWs with up-state of OFC slow oscillations

These results indicate that SPW-associated synchronized discharges of APC neurons occur in phase with the up-state of the OFC and that these APC neurons tend to show reduced activity during the down-state of the OFC (Fig. 1). Given that OFC neurons show enhanced spike activity during the OFC up-state, these results suggest that the up-state of the OFC provides a time window for enhanced interaction between OFC neurons and APC neurons. Consistent with this notion, about 45% of recorded OFC neurons showed enhanced spike discharges in synchrony with APC-SPWs, a period in which numerous APC neurons show synchronized discharges (Manabe et al. 2011).

This interaction between APC and OFC can be mediated by direct and indirect axonal connections between these areas. First, APC and OFC have mutual direct axonal connections (Illig 2005; Neville and Haberly 2004; Ray and Price 1992) (Fig. 9). Pyramidal cells in the APC give rise to a direct feed-forward axon projection to the OFC, while pyramidal cells in the OFC send a direct top-down projection to the deep layer (layer III) of the APC (Illig 2005). Given that APC-SPWs are generated by excitatory

synaptic inputs to the deep layer of the APC (Manabe et al. 2011), it is possible that the top-down signal transmission from the OFC to the APC may contribute to their generation. Second, APC and OFC may interact through indirect axonal connections via the mediodorsal nucleus of the thalamus (MD). Pyramidal cells in the deep layers of the APC project axons to the MD (Neville and Haberly 2004; Ray and Price 1992), and the thalamocortical neurons in the MD send axons to the OFC (Fig. 9). Because APC-SPWs are considered to be generated by excitatory synaptic inputs to the deep layer of APC, the synchronized activity of APC neurons during APC-SPWs might be transmitted to the OFC via these indirect transthalamic pathways. Finally, neurons in the endopiriform nucleus (En) receive axonal inputs from APC pyramidal cells and project axons to the OFC (Behan and Haberly 1999) raising the possibility that En neurons might be involved in the interaction between the APC and OFC during APC-SPWs.

Detailed examination of the timing of APC-SPW occurrence with reference to the time course of OFC up-state showed that APC-SPWs occur preferentially either at the beginning of up-state shortly after the down-to-up transition of OFC slow-wave activity, or at the end of up-state shortly before the up-to-down transition. This observation suggests that enhanced interactions between APC neurons and OFC neurons occur at specific time windows shortly after the down-to-up transition and shortly before the

up-to-down transition of OFC slow-wave activity. The up-state of the neocortex slow oscillations provides the time window for the generation of not only APC-SPWs but also spindle activities during sleep. During slow wave sleep, the neocortex shows two types of spindle that differ in frequency and generation area: fast spindles with peak frequencies between 12 to 15 Hz and widespread distribution over the central and parietal areas, and slow spindles with peak frequencies between 9 and 12 Hz and focused distribution over the frontal cortical areas (Anderer et al. 2001; De Gennaro and Ferrara 2003; Mölle et al. 2011; Terrier and Gottesmann 1978). Interestingly, while fast spindles in the central and parietal areas are synchronized with the down-to-up transition of slow-wave activity, the slow spindles in the frontal cortical areas occur in association with the up-to-down transition (Mölle et al. 2011). These results suggest that during up-states, the time windows shortly after the down-to-up transition and shortly before the up-to-down transition play distinct functional roles in thalamo-cortical and cortico-cortical communications. The emergence of down-to-up transition in the neocortex may drive thalamic spindle generation and mediate communications between the central and parietal cortices and thalamus at the early phase of up-state (Anderer et al. 2001; Mölle et al. 2011). In contrast, the generation of slow spindles during up-to-down transitions may originate in the frontal cortex areas at the late phase of

up-state (Anderer et al. 2001; Mölle et al. 2011), raising the possibility that the slow spindles might be involved in the generation of down-state.

Consistent with the two types of spindle, my study identified two types of APC-SPW: initial phase APC-SPWs, which occur during the initial phase of up-state shortly after the down-to-up transition, and late phase APC-SPWs, which occur during the last part of the up-state shortly before the up-to-down transition. In analogy with the functional difference in the two types of spindles, I speculate that initial phase APC-SPWs differ from late phase APC-SPWs in the functional meaning of APC-OFC communication. At the initial phase of up-state, initial phase APC-SPWs may drive OFC neurons or synchronized activity of OFC neurons drive the initial phase APC-SPWs to generate and maintain up-state in both the OFC and APC. At the late phase of up-state, on the other hand, late phase APC-SPWs might mediate distinct interactions between the APC and OFC to generate a synchronized down-state in the OFC and APC. Consistent with this notion, recent experimental results revealed that the up-to-down transition (onset of down-state) is more synchronous between remote populations of neurons than the down-to-up transition (onset of up-state) (Chen et al. 2012), suggesting the presence of a neural circuit mechanism that actively generates the down-state synchronously across the OFC and APC. Further studies are necessary to elucidate the functional roles of

APC-OFC communication at the initial- and late-phases of up-state.

Grouping influence of frontal cortex slow-wave activity on olfactory cortex SPWs

Hippocampal SPW/ripple activities and thalamic spindle activities occur in temporal coordination with neocortical up-states during slow-wave sleep (Isomura et al. 2006; Mölle and Born 2011; Siapas and Wilson 1998; Sirota et al. 2003; Steriade et al. 1993a, 1993b, 1993c). Neocortical fast oscillatory activity (20–60 Hz) also occurs in synchrony with the up-states (Steriade 2006). The present results indicate that olfactory cortex SPW activities also occur in temporal coordination with the neocortical up-state. My results thus support the idea that neocortical up-state provides key time windows for the sleep-time communications across large-scale neuronal networks that involve olfactory cortex areas, hippocampal regions, thalamic nuclei, and neocortex areas, including the frontal cortex.

It has been shown that the firing pattern of hippocampal CA1 neurons that occurs during awake exploratory behavior appears to be replayed in association with hippocampal SPW/ripple events during the up-state of slow-wave activity in the neocortex (Ji and Wilson 2007). Coordinated activity among hippocampal SPW/ripple events and the neocortical up-state is hypothesized to play a role in the process of the

memory consolidation (Girardeau et al. 2009; Ji and Wilson 2007; Siapas and Wilson 1998; Sirota et al. 2003). My present results suggest the possibility that SPW-associated synchronized activities of APC neurons provide the means to communicate widely with the OFC during the up-state. I speculate that coordinated activities of the APC and OFC during the OFC up-state of slow oscillation might represent the reactivation of neuronal firing patterns that occurred during wakefulness, and that the coordination between APC-SPWs and OFC up-state may be associated with olfactory memory consolidation.

This study showed that not only APC-SPWs but also PPC-SPWs and OB-SPWs occurred during the early and late phases of the up-state of both the OFC and mPFC. In other words, SPW events in large-scale networks of olfactory areas are coordinated in precise time windows during the up-states of the large-scale networks of the frontal cortex. This suggests that many olfactory cortex areas, neocortex areas, thalamic regions and hippocampal regions communicate with each other during the early and late phases of the up-state of neocortical slow-wave activity. Further studies are necessary to elucidate the functional roles of this communication among the large-scale networks of the forebrain during slow-wave sleep.

Acknowledgements

I am sincerely grateful to Professor Kensaku Mori for supervision and continuous supports during this study. I greatly appreciate Dr. Hiroyuki Manabe for technical support and a number of valuable suggestions. I thank all the members of Department of Molecular and Cellular Physiology, Graduate School of Medicine, the University of Tokyo for valuable suggestions and discussions. I also would like to express my gratitude to Professor Masanobu Kano for support to continue this study.

References

Anderer P, Klösch G, Gruber G, Trenker E, Pascual-Marqui RD, Zeitlhofer J, Barbanoj MJ, Rappelsberger P, and Saletu B. Low-resolution brain electromagnetic tomography revealed simultaneously active frontal and parietal sleep spindle sources in the human cortex. *Neuroscience* 103: 581–592, 2001.

Behan M, and Haberly LB. Intrinsic and efferent connections of the endopiriform nucleus in rat. *J Comp Neurol* 408: 532–548, 1999.

Chen JY, Chauvette S, Skorheim S, Timofeev I, and Bazhenov M. Interneuron-mediated inhibition synchronizes neuronal activity during slow oscillation. *J Physiol* 590: 3987–4010, 2012.

Contreras D, and Steriade M. Cellular basis of EEG slow rhythms: a study of dynamic corticothalamic relationships. *J Neurosci* 15: 604–622, 1995.

Courtiol E, and Wilson DA. Thalamic olfaction: characterizing odor processing in the mediodorsal thalamus of the rat. *J Neurophysiol* 111: 1274–1285, 2014.

De Gennaro L, and Ferrara M. Sleep spindles: an overview. *Sleep Med Rev* 7: 423–440, 2003.

Fu W, Sugai T, Yoshimura H, and Onoda N. Convergence of olfactory and gustatory connections onto the endopiriform nucleus in the rat. *Neuroscience* 126: 1033–1041, 2004.

Girardeau G, Benchenane K, Wiener SI, Buzsáki G, and Zugaro MB. Selective suppression of hippocampal ripples impairs spatial memory. *Nat Neurosci* 12: 1222–1223, 2009.

Harris KD, Henze DA, Csicsvari J, Hirase H, and Buzsáki G. Accuracy of tetrode spike separation as determined by simultaneous intracellular and extracellular measurements. *J Neurophysiol* 84: 401–414, 2000.

Illig KR. Projections from orbitofrontal cortex to anterior piriform cortex in the rat suggest a role in olfactory information processing. *J Comp Neurol* 488: 224–231, 2005.

Isomura Y, Sirota A, Özen S, Montgomery S, Mizuseki K, Henze DA, and Buzsáki G. Integration and segregation of activity in entorhinal-hippocampal subregions by neocortical slow oscillations. *Neuron* 52: 871–882, 2006.

Ji D, and Wilson MA. Coordinated memory replay in the visual cortex and hippocampus during sleep. *Nat Neurosci* 10: 100–107, 2007.

Komano-Inoue S, Manabe H, Ota M, Kusumoto-Yoshida I, Yokoyama TK, Mori K, and Yamaguchi M. Top-down inputs from the olfactory cortex in the postprandial

period promote elimination of granule cells in the olfactory bulb. *Eur J Neurosci* 40: 2724–2733, 2014.

Krettek JE, and Price JL. The cortical projections of the mediodorsal nucleus and adjacent thalamic nuclei in the rat. *J Comp Neurol* 171: 157–191, 1977.

Lipowska M, Kowiański P, Majak K, Jagalska-Majewska H, and Moryś J. The connections of the endopiriform nucleus with the insular claustrum in the rat and rabbit. *Folia Morphol (Warsz)* 59: 77–83, 2000.

Manabe H, Kusumoto-Yoshida I, Ota M, and Mori K. Olfactory cortex generates synchronized top-down inputs to the olfactory bulb during slow-wave sleep. *J Neurosci* 31: 8123–8133, 2011.

Massimini M, Huber R, Ferrarelli F, Hill S, and Tononi G. The sleep slow oscillation as a traveling wave. *J Neurosci* 24: 6862–6870, 2004.

Mölle M, Bergmann TO, Marshall L, and Born J. Fast and slow spindles during the sleep slow oscillation: disparate coalescence and engagement in memory processing. *Sleep* 34: 1411–1421, 2011.

Mölle M, and Born J. Slow oscillations orchestrating fast oscillations and memory consolidation. *Prog Brain Res* 193: 93–110, 2011.

Mori K, Manabe H, Narikiyo K, and Onisawa N. Olfactory consciousness and gamma oscillation couplings across the olfactory bulb, olfactory cortex, and orbitofrontal cortex. *Front Psychol* 4: 743, 2013.

Murphy M, Riedner BA, Huber R, Massimini M, Ferrarelli F, and Tononi G. Source modeling sleep slow waves. *Proc Natl Acad Sci U S A* 106: 1608–1613, 2009.

Narikiyo K, Manabe H, and Mori K. Sharp wave-associated synchronized inputs from the piriform cortex activate olfactory tubercle neurons during slow-wave sleep. *J Neurophysiol* 111: 72–81, 2014.

Neville KR, and Haberly LB. Olfactory cortex. In: *The synaptic organization of the brain* (5the ed), edited by Shepherd GM. New York: Oxford University Press, 2004.

Ray JP, and Price JL. The organization of the thalamocortical connections of the mediodorsal thalamic nucleus in the rat, related to the ventral forebrain-prefrontal cortex topography. *J Comp Neurol* 323: 167–197, 1992.

Siapas AG, and Wilson MA. Coordinated interactions between hippocampal ripples and cortical spindles during slow-wave sleep. *Neuron* 21: 1123–1128, 1998.

Sirota A, Csicsvari J, Buhl D, and Buzsáki G. Communication between neocortex and hippocampus during sleep in rodents. *Proc Natl Acad Sci U S A* 100: 2065–2069, 2003.

Steriade M. Grouping of brain rhythms in corticothalamic systems. *Neuroscience* 137: 1087–1106, 2006.

Steriade M, and Contreras D. Relations between cortical and thalamic cellular events during transition from sleep patterns to paroxysmal activity. *J Neurosci* 15: 623–642, 1995.

Steriade M, Contreras D, Curró Dossi R, and Nuñez A. The slow (< 1 Hz) oscillation in reticular thalamic and thalamocortical neurons: scenario of sleep rhythm generation in interacting thalamic and neocortical networks. *J Neurosci* 13: 3284–3299, 1993a.

Steriade M, Gloor P, Llinás RR, Lopes de Silva FH, and Mesulam MM. Report of IFCN Committee on Basic Mechanisms. Basic mechanisms of cerebral rhythmic activities. *Electroencephalogr Clin Neurophysiol* 76: 481–508, 1990.

Steriade M, Nuñez A, and Amzica F. Intracellular analysis of relations between the slow (< 1 Hz) neocortical oscillation and other sleep rhythms of the electroencephalogram. *J Neurosci* 13: 3266–3283, 1993b.

Steriade M, Nuñez A, and Amzica F. A novel slow (< 1 Hz) oscillation of neocortical neurons in vivo: depolarizing and hyperpolarizing components. *J Neurosci* 13: 3252–3265, 1993c.

Steriade M, Timofeev I, and Grenier F. Natural waking and sleep states: a view from inside neocortical neurons. *J Neurophysiol* 85: 1969–1985, 2001.

Terrier G, and Gottesmann CL. Study of cortical spindles during sleep in the rat. *Brain Res Bull* 3: 701–706, 1978.

Timofeev I, Grenier F, and Steriade M. Disfacilitation and active inhibition in the neocortex during the natural sleep-wake cycle: an intracellular study. *Proc Natl Acad Sci U S A* 98: 1924–1929, 2001.

Tsuno Y, Kashiwadani H, and Mori K. Behavioral state regulation of dendrodendritic synaptic inhibition in the olfactory bulb. *J Neurosci* 28:9227-9238, 2008.

Vyazovskiy VV, Olcese U, Hanlon EC, Nir Y, Cirelli C, and Tononi G. Local sleep in awake rats. *Nature* 472: 443–447, 2011.

Figure legends

Fig. 1 Coordinated occurrence of OFC down-state and APC down-state during slow-wave sleep.

A: Simultaneous recordings of local field potential (LFP) with multiunit spike activity (MUA) from the orbitofrontal cortex (OFC) and anterior piriform cortex (APC), together with the animal's respiration (Resp). Upward swing in the respiration monitor indicates inhalation. Vertical bars on the OFC-LFP indicate the peak of depth-positive potential (tentative down-state) in the OFC. Arrows show APC-SPWs. B: Averaged time course of OFC-LFP aligned in reference to the peak of the OFC down-state (top trace). Bottom histograms show the peri-down-state time histogram of the single cell spike activity of three simultaneously recorded OFC neurons. The horizontal dashed line indicates the statistical threshold level (2 SDs below the background firing frequency) for detecting reduced activity. Asterisks indicate that OFC unit activity decreases significantly during OFC down-states. C: Filtered traces of OFC-LFP and APC-LFP in Fig. 1A. Each LFP recording was down-sampled to 100 Hz and low-pass filtered at 4 Hz. D: Mean coherence (n = 8 experiments from 3 rats, 2 or 3 experiments per rat) between OFC-LFP and APC-LFP (solid line, ± SD; dashed line). E: Averaged time

course of OFC-LFP aligned in reference to the peak of OFC down-state (top trace). Bottom histograms show peri-down-state time histogram of single-cell firings of three simultaneously recorded APC neurons. The horizontal dashed line indicates the statistical threshold level (2 SDs below the background firing frequency) for detecting the reduced activity. Asterisks indicate that APC unit activity decreases significantly during OFC down-states.

Fig. 2 Estimation of OFC down-state based on configuration of the OFC local field potential.

A: Local field potentials (LFPs) in the OFC, filtered traces of the OFC-LFP, and spike histogram of simultaneously recorded OFC neurons. Horizontal black dashed line shows the mean of the filtered LFP. Horizontal colored dashed lines show the mean + various SDs of the filtered OFC-LFP (blue, 1 SD; green, 1.5 SDs; red, 2 SDs; yellow, 2.5 SDs). B: Peri-down-states time histogram of OFC multiunits (all 22 cells in Fig. C). Tentative peak of the down-state is shown at 0 sec. Down-states were detected in four different ways with distinct threshold levels (blue, mean + 1 SD; green, mean + 1.5 SDs; red, mean + 2 SDs; yellow, mean + 2.5 SDs). C: Peri-down-state time histogram of 22 simultaneously recorded single neurons in the OFC. The threshold for detecting

tentative peak of down-states was set as the mean + 2 SDs (2 SD of Fig. 2, A and B). Vertical red dashed line shows the tentative peak of the OFC down state.

Fig. 3 Occurrence of APC-SPWs shortly after the down-to-up transition and shortly before the up-to-down transition of OFC slow-wave activity.

A: Superimposition of 10 traces of OFC down-states (upper traces) aligned in reference to the peak of OFC down-states. Gray trace is the averaged time course of OFC-LFP during down-states. Lower traces show APC-LFPs with APC-SPWs superimposed in reference to the peak of OFC down-state. Arrows indicate the trough of APC-SPW. B: Averaged time course of OFC-LFP during down-states (top trace) and peri-down-state time histogram of the troughs of APC-SPWs (bottom histogram). C: Comparison of the frequency of APC-SPW events between up-state period and down-state period. Data represent mean ± SD (n = 8 experiments from 3 rats, 2 or 3 experiments per rat). ***, $p < 0.001$ (paired t-test).

Fig. 4 APC-SPWs occurring at the two distinct phases of the OFC up-state.

A: Timing of APC-SPW occurrence in reference to each cycle of OFC slow-wave activity. A convenience sample of 15 traces of OFC slow-wave cycles with different

duration was plotted. Each trace was aligned with the start of the OFC up-state (the peak of the preceding OFC down-state, vertical dashed line, 0 s). Short black lines indicate the end of up-state (the time point at –90 msec before the peak of subsequent down-state). Gray lines show the time of APC-SPW occurrence. B: An enlarged example of OFC-LFP and APC-LFP that corresponds to the trace #7 in Fig. 4A. The start of the OFC up-state (the peak of the preceding down-state) was set to 0 s (dashed line). The short black line shows the end of up-state (the time point at –90 msec before the peak of subsequent down-state). Gray line shows APC-SPW. C: Phase histogram of APC-SPWs with reference to the cycle of OFC up-state (n = 8 experiments from 3 rats, 2 or 3 experiments per rat). One cycle of OFC up-state is divided into 360° (with 12° bins). The start of up-state (peak of the preceding OFC down-state) was set to 0°, and the end of up-state (the time point at –90 msec before the peak of subsequent down-state) was set to 360°. Phase I, Phase II and Phase III indicate the initial one-third (0°–120°), middle one-third (120°–240°), and the later one-third (240°–360°) of the up-state period respectively. Horizontal gray dashed line indicates mean + 2 SDs of the APC-SPW probability during Phase II. Because APC-SPW probability during Phase I and that during III exceeded this line, the probability of APC-SPW occurrence in both Phase I and that in Phase III were considered to be significantly higher than that in

Phase II. Data represent mean ± SD (n = 8 experiments from 3 rats, 1 or 2 experiments per rat).

Fig. 5 Tendency of APC-SPWs to occur more frequently around the global OFC down-state than around the local OFC down-state.

A: Simultaneous recordings of local field potentials (LFPs) and multiunit activity (MUA) in the orbitofrontal cortex (OFC) and the anterior piriform cortex (APC) during the global OFC down-state (left column) and local OFC down-state (right column). B: Left column shows peri-global OFC down-state time histograms of OFC multiunit (MU) activities (top histogram) and APC multiunit (MU) activities (bottom histogram). Right column shows peri-local OFC down-state time histograms of OFC multiunit (MU) activities (top histogram) and APC multiunit (MU) activities (bottom histogram). C: Comparison of multiunit (MU) activities among up-state period, global down-state period, local down-state period (OFC multiunits, left; APC multiunits, right). Data represent mean ± SD (n = 8 experiments from 3 rats, 2 or 3 experiments per rat). *, $p < 0.05$; ***, $p < 0.001$ (one-way ANOVA with post hoc Tukey test). D: Peri-global OFC down-state time histogram of APC-SPWs (left) and peri-local OFC down-state time histogram of APC-SPWs (right). E: Frequency of APC-SPW occurrence around the

global (left) and local (right) OFC down-states (n = 8 experiments from 3 rats, 2 or 3 experiments per rat). ***, $p < 0.001$ (paired t-test).

Fig. 6 OFC neurons that showed enhanced spike discharges in synchrony with the APC-SPWs.

Averaged time course of APC-SPW (top trace) and peri-SPW time histogram of three simultaneously recorded OFC neurons (bottom histograms). Horizontal dashed line indicates the statistical threshold level (3 SDs above background firing frequency) for the detection of APC-SPW-associated enhanced discharges. Asterisks indicate that OFC unit activity increased significantly during the APC-SPW.

Fig. 7 Coordinated slow-wave activities in wide areas of the prefrontal cortex and central olfactory system.

A: Simultaneous recordings of local field potentials (LFPs) in the orbitofrontal cortex (OFC), medial prefrontal cortex (mPFC), anterior piriform cortex (APC), posterior piriform cortex (PPC), and olfactory bulb (OB). Vertical bars on the OFC-LFP and mPFC-LFP indicate the peak of depth-positive potential (tentative down-state) in the OFC and mPFC. Arrows show APC-SPWs, PPC-SPWs and OB-SPWs. B: Filtered

traces of OFC-LFP, mPFC-LFP, APC-LFP, PPC-LFP and OB-LFP. Each LFP was down-sampled to 100 Hz and low-pass filtered at 4 Hz. C: Averaged coherence of slow-wave activity between OFC and mPFC, OFC and APC, OFC and PPC, OFC and OB, mPFC and APC, mPFC and PPC, and mPFC and OB. Data represent mean ± SD (n = 3 rats). **, $p < 0.01$; ***, $p < 0.001$; n.s., not significant (one-way ANOVA with post hoc Tukey test).

Fig. 8 Occurrence of APC-SPWs, PPC-SPWs and OB-SPWs in synchrony with up-states of both OFC and mPFC.

A: Averaged time course of OFC down-states (left, top trace) and mPFC down-states (right, top trace) and peri-down-state time histogram of APC-SPWs, PPC-SPWs, and OB-SPWs (bottom histograms). B: Phase histogram of APC-SPWs, PPC-SPWs, and OB-SPWs with the cycle of OFC up-state (left column) and mPFC up-state (right column). The start of up-state (the peak of preceding down-state) was set to 0°. The end of up-state (–90 msec before the subsequent down-state) was set to 360°. Phase I, Phase II and Phase III indicate the initial one-third (0°–120°), the middle one-third (120°–240°), and the later one-third (240°–360°) of each up-state period, respectively. Horizontal dashed line indicates mean + 2 SDs of the APC-SPW, PPC-SPW and

OB-SPW probability during Phase II. If the SPW probability in Phase I or that in Phase III exceeded this line, I considered that the SPW generation increased significantly in Phase I or Phase III. Data represent mean ± SD (n = 3 rats). C: Peri-OFC down-state time histogram of averaged probability of mPFC down-state events. The averaged probability in each bin was calculated for all the data from different data and from different animals (n = 4 rats).

Fig. 9 Schematic diagram illustrating possible pathways for communication between the APC and the OFC during slow-wave sleep.

Direct axonal connections: Pyramidal cells (Py) in the anterior piriform cortex (APC) project axons directly to the orbitofrontal cortex (OFC), while pyramidal cells in the OFC send top-down axons to the deep layer of the APC. Indirect connections: APC pyramidal cells project axons to the mediodorsal nucleus (MD) of the thalamus and thalamocortical neurons (TC) in the MD project axons to the OFC. APC neurons also project axons to the endopiriform nucleus (En) and multipolar cells (MPC) in the En send axons to the OFC. For simplicity, local inhibitory interneurons are omitted from this diagram. I, II, III, layers in the APC; I, II/III, V/VI, layers in the OFC.

Figure 1

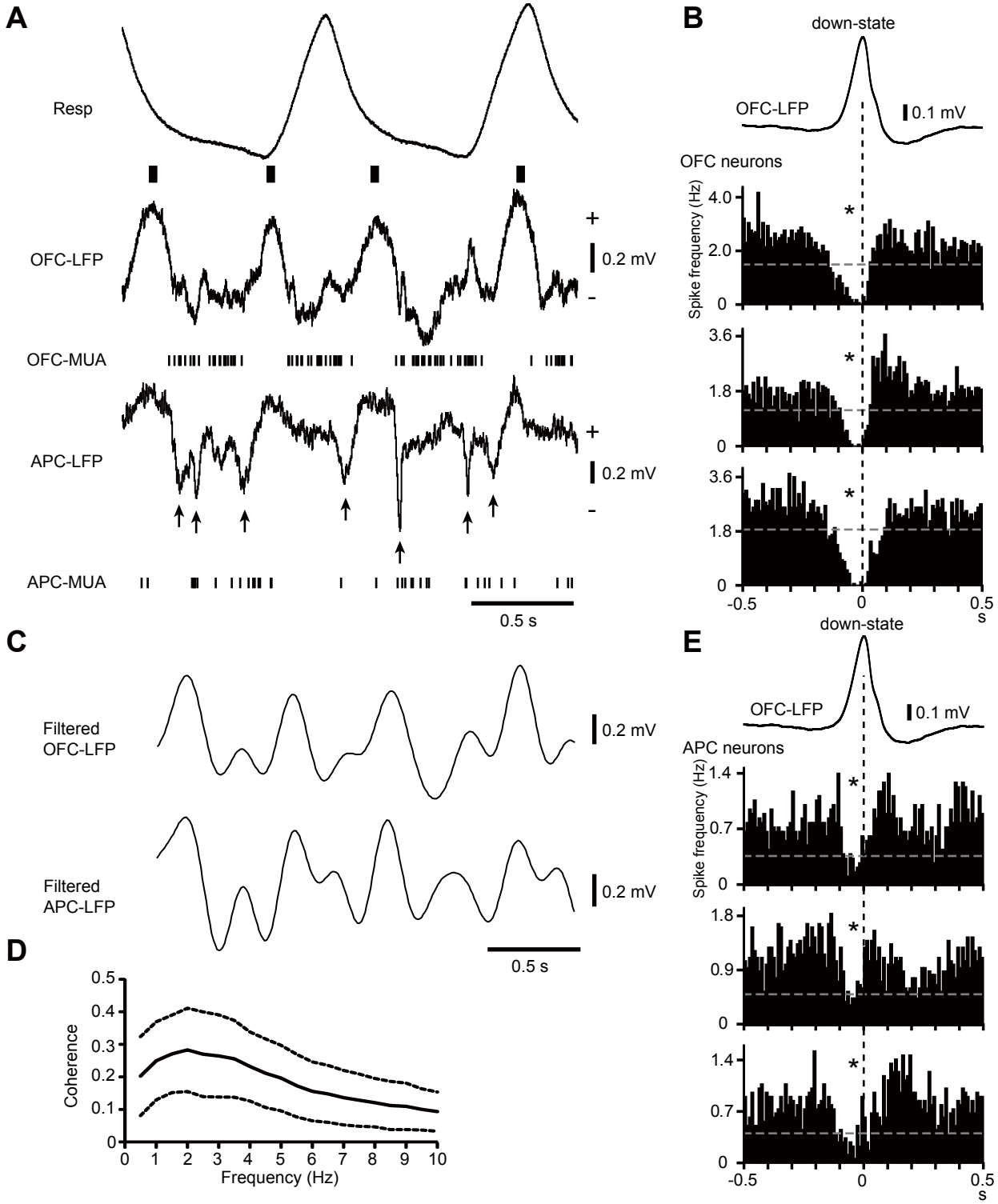
A
Resp
OFC-LFP
OFC-MUA
APC-LFP
APC-MUA
0.2 mV
0.5 s
B
down-state
OFC-LFP
0.1 mV
OFC neurons
Spike frequency (Hz)
4.0
2.0
0
3.6
1.8
-0.5
0
0.5
s
C
Filtered OFC-LFP
Filtered APC-LFP
0.2 mV
0.5 s
D
Coherence
Frequency (Hz)
E
down-state
OFC-LFP
0.1 mV
APC neurons
Spike frequency (Hz)
1.4
0.7
1.8
0.9

Figure 2

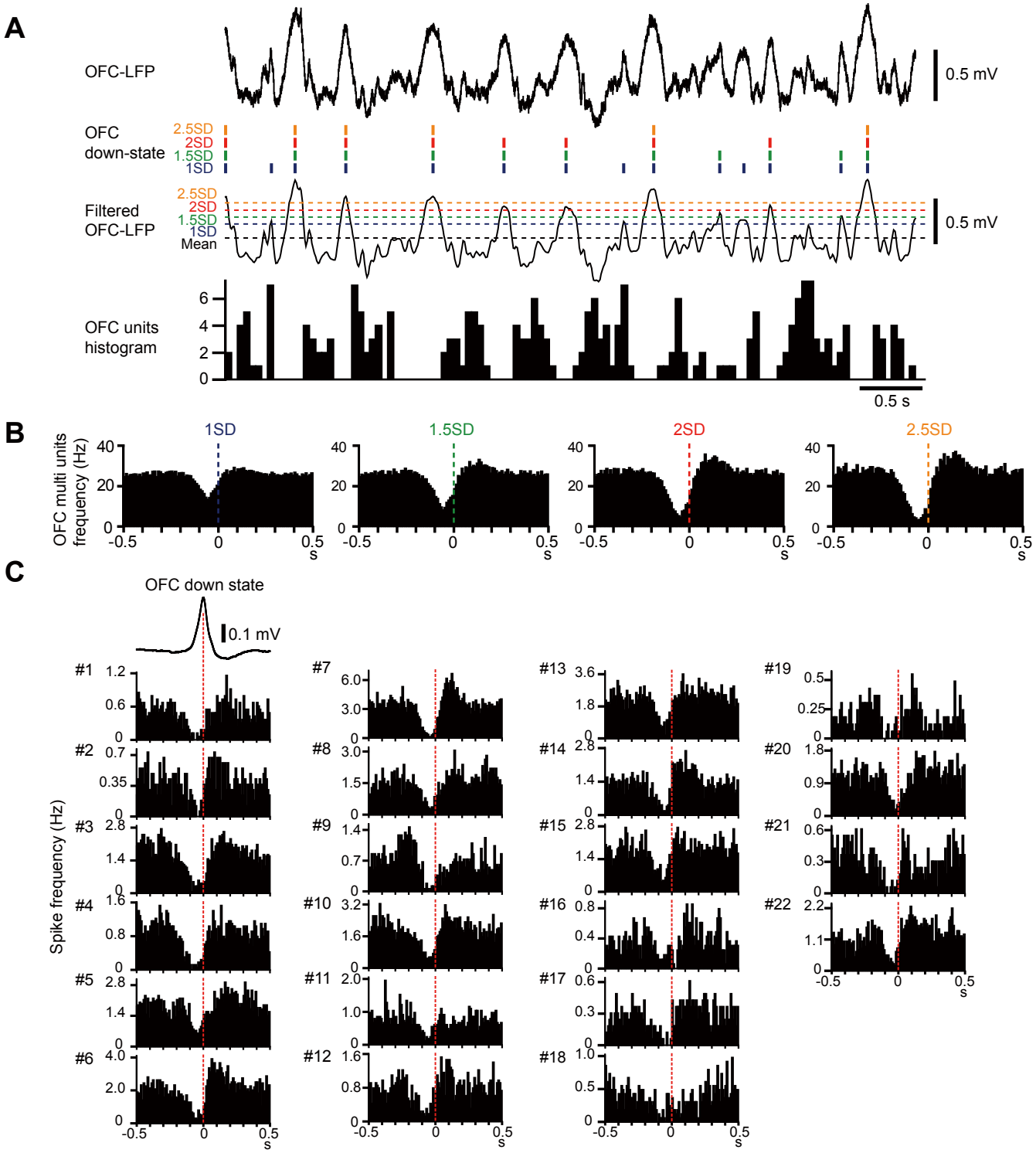
A
OFC-LFP
0.5 mV
OFC down-state
2.5SD
2SD
1.5SD
1SD
Filtered OFC-LFP
Mean
0.5 mV
OFC units histogram
0.5 s
B
1SD
1.5SD
2SD
2.5SD
OFC multi units frequency (Hz)
s
C
OFC down state
0.1 mV
Spike frequency (Hz)
#1
#2
#3
#4
#5
#6
#7
#8
#9
#10
#11
#12
#13
#14
#15
#16
#17
#18
#19
#20
#21
#22

Figure 3

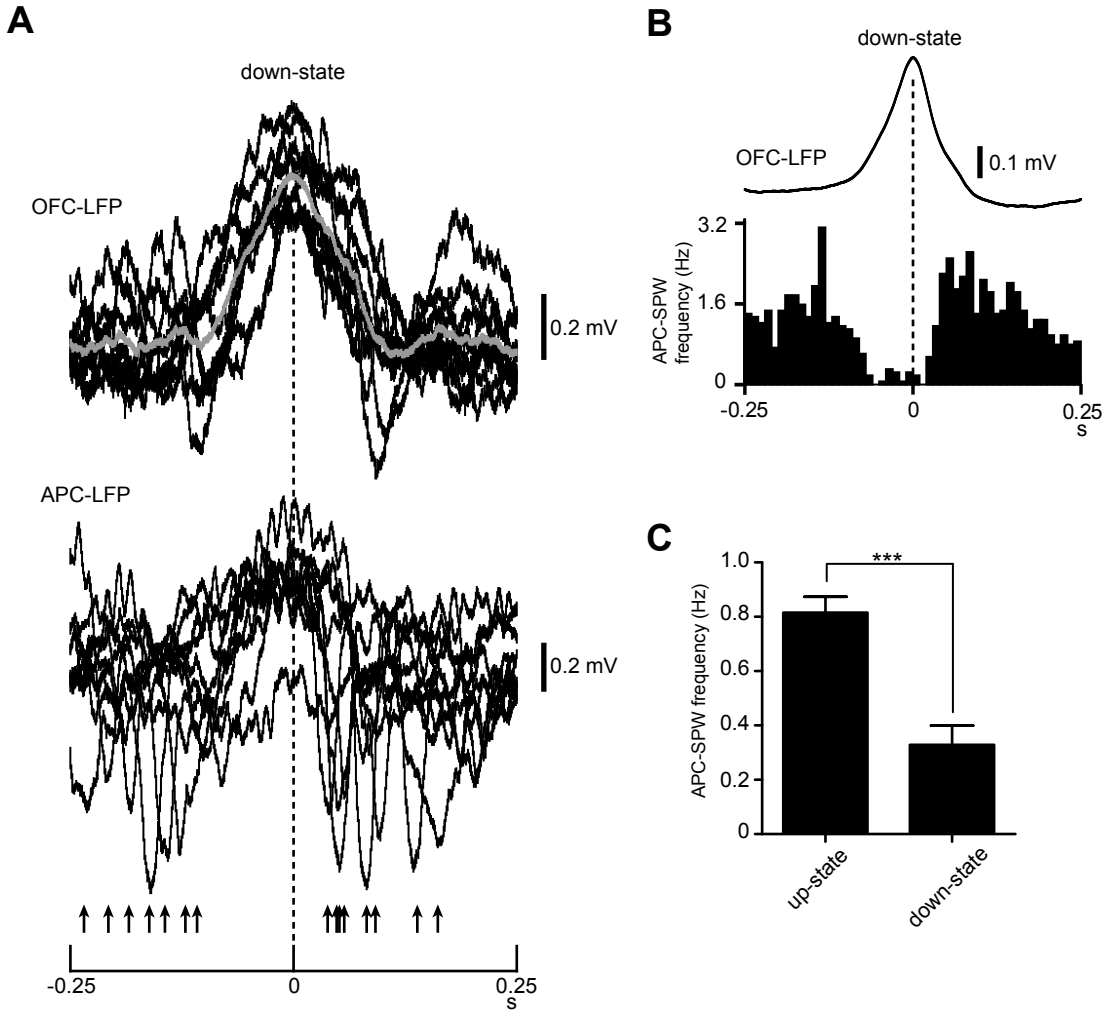
A
down-state
OFC-LFP
0.2 mV
APC-LFP
0.2 mV
-0.25
0
0.25
s
B
down-state
OFC-LFP
0.1 mV
APC-SPW frequency (Hz)
3.2
1.6
0
-0.25
0
0.25
s
C
APC-SPW frequency (Hz)
1.0
0.8
0.6
0.4
0.2
0
***
up-state
down-state

Figure 4

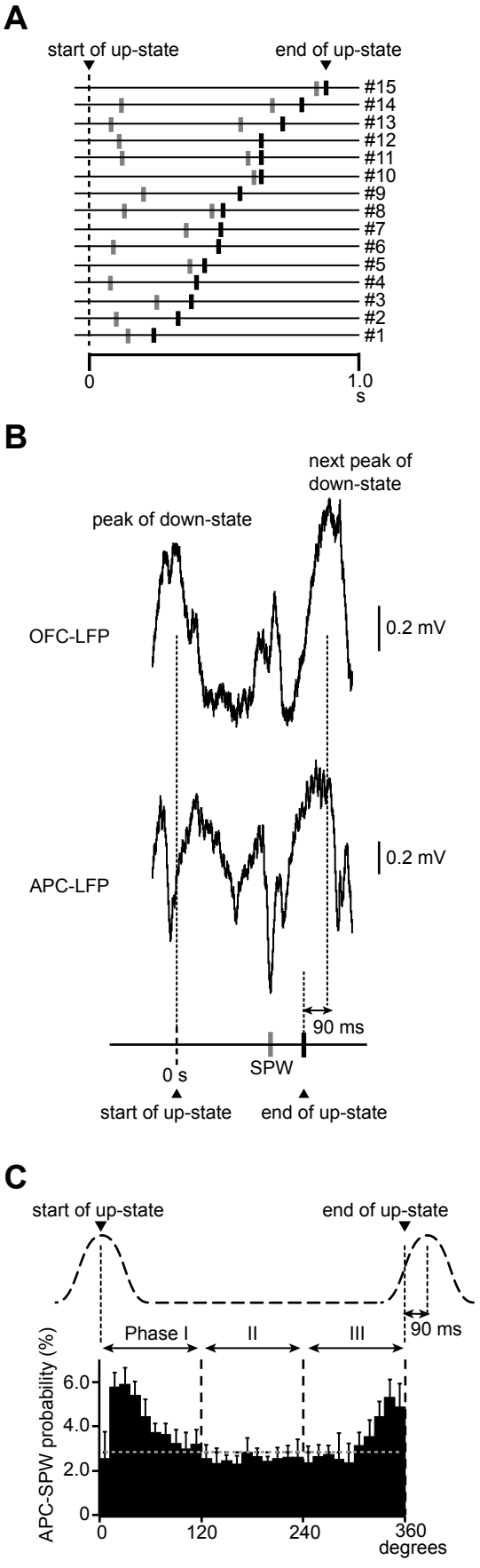
A
start of up-state
end of up-state
#15
#14
#13
#12
#11
#10
#9
#8
#7
#6
#5
#4
#3
#2
#1
0
1.0
s
B
next peak of
down-state
peak of down-state
OFC-LFP
0.2 mV
APC-LFP
0.2 mV
90 ms
SPW
0 s
start of up-state
end of up-state
C
start of up-state
end of up-state
90 ms
Phase I
II
III
APC-SPW probability (%)
6.0
4.0
2.0
0
0
120
240
360
degrees

Figure 5

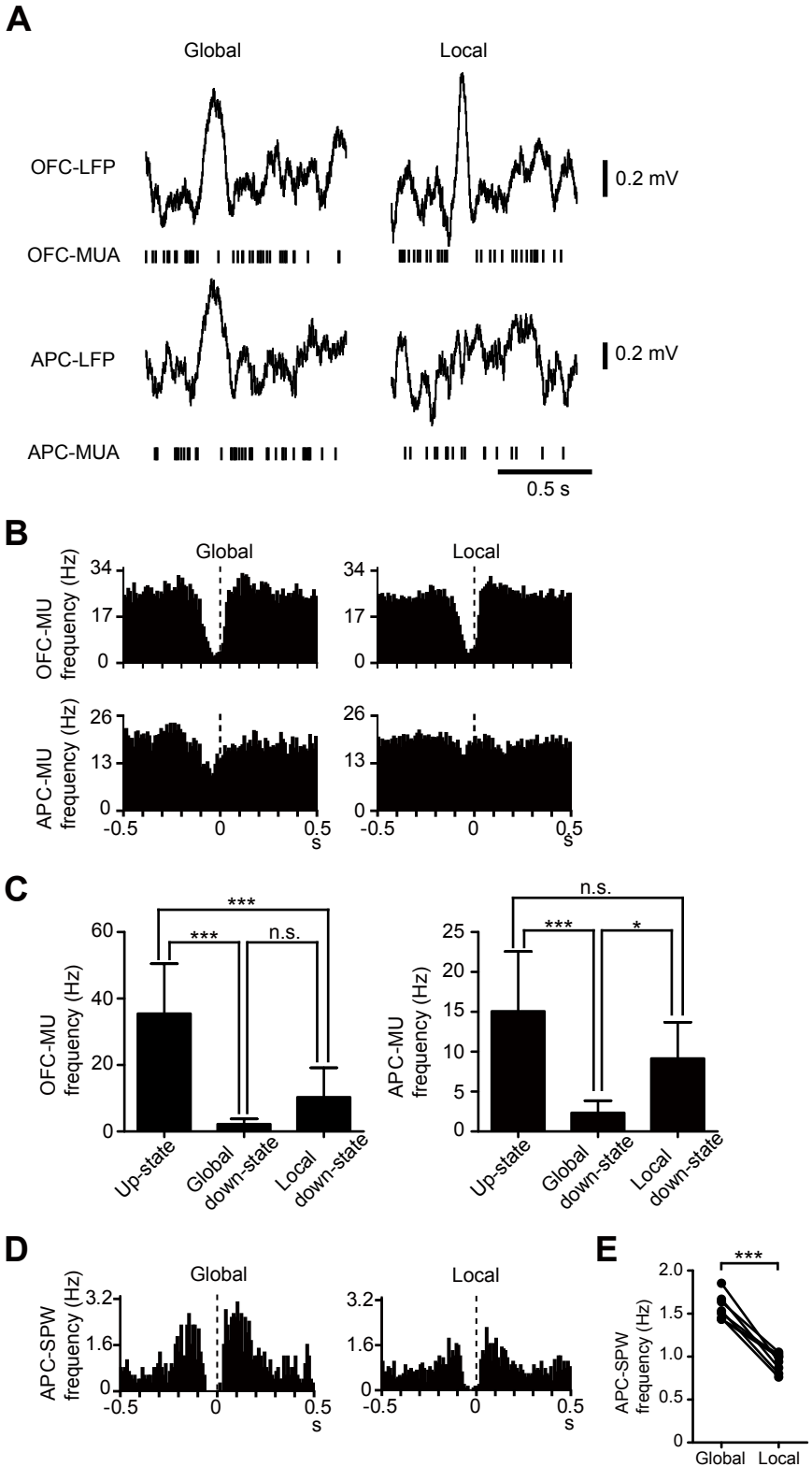
A
Global
Local
OFC-LFP
0.2 mV
OFC-MUA
APC-LFP
0.2 mV
APC-MUA
0.5 s
B
Global
Local
OFC-MU frequency (Hz)
34
17
0
APC-MU frequency (Hz)
26
13
0
-0.5
0
0.5
s
C
***
***
n.s.
OFC-MU frequency (Hz)
60
40
20
0
Up-state
Global down-state
Local down-state
n.s.
***
*
APC-MU frequency (Hz)
25
20
15
10
5
0
D
Global
Local
APC-SPW frequency (Hz)
3.2
1.6
0
E
***
APC-SPW frequency (Hz)
2.0
1.5
1.0
0.5
0
Global
Local

Figure 6

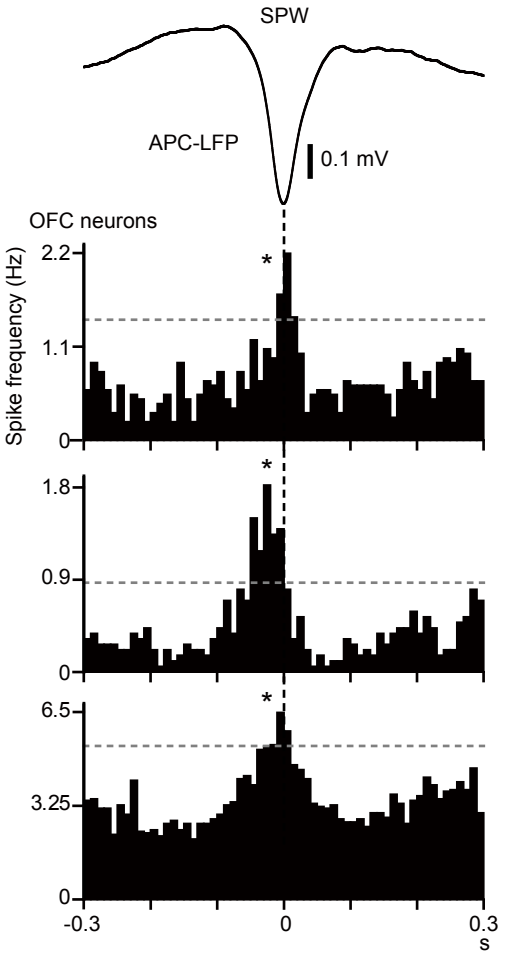
SPW
APC-LFP
0.1 mV
OFC neurons
Spike frequency (Hz)
2.2
1.1
0
1.8
0.9
0
6.5
3.25
0
*
*
*
-0.3
0
0.3
s

Figure 7

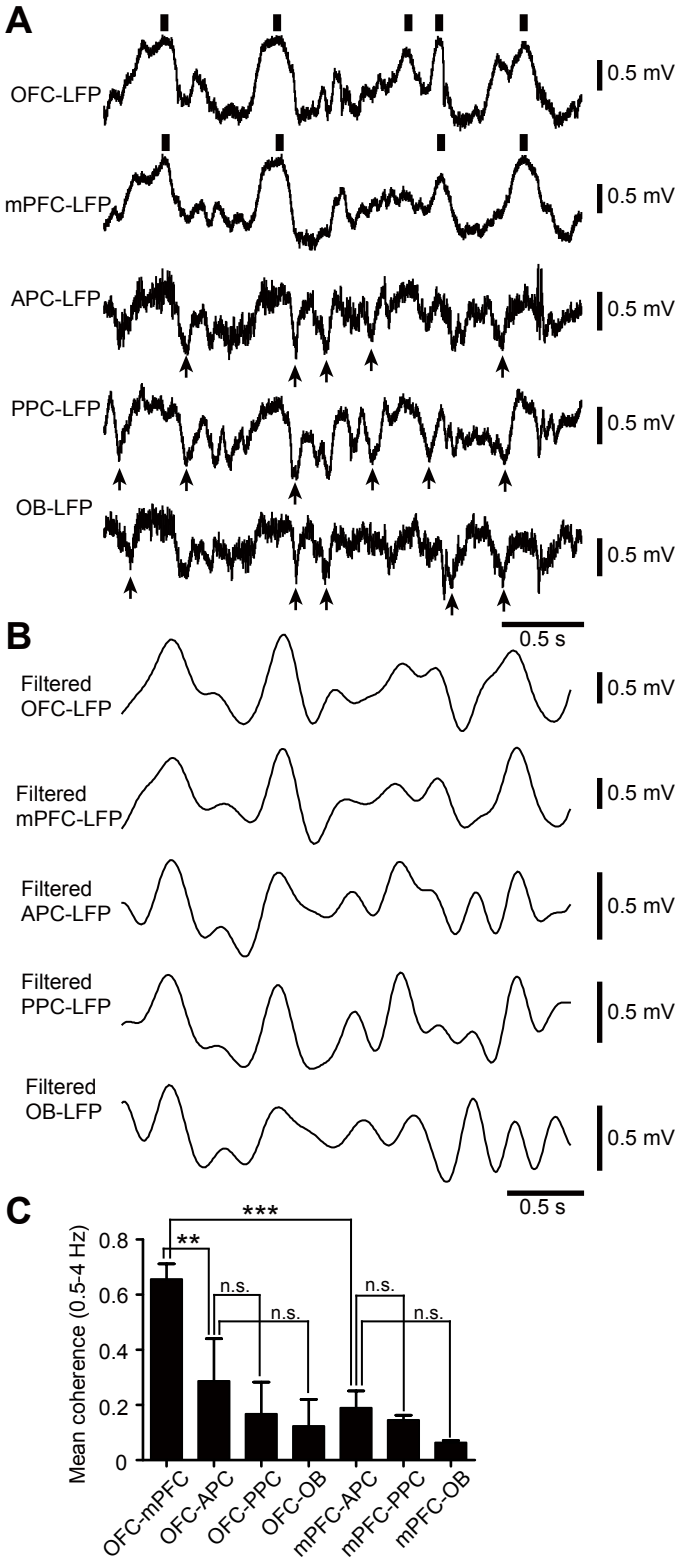
A
OFC-LFP
mPFC-LFP
APC-LFP
PPC-LFP
OB-LFP
0.5 mV
0.5 s
B
Filtered OFC-LFP
Filtered mPFC-LFP
Filtered APC-LFP
Filtered PPC-LFP
Filtered OB-LFP
C
Mean coherence (0.5-4 Hz)
0
0.2
0.4
0.6
0.8
**
***
n.s.
OFC-mPFC
OFC-APC
OFC-PPC
OFC-OB
mPFC-APC
mPFC-PPC
mPFC-OB

Figure 8

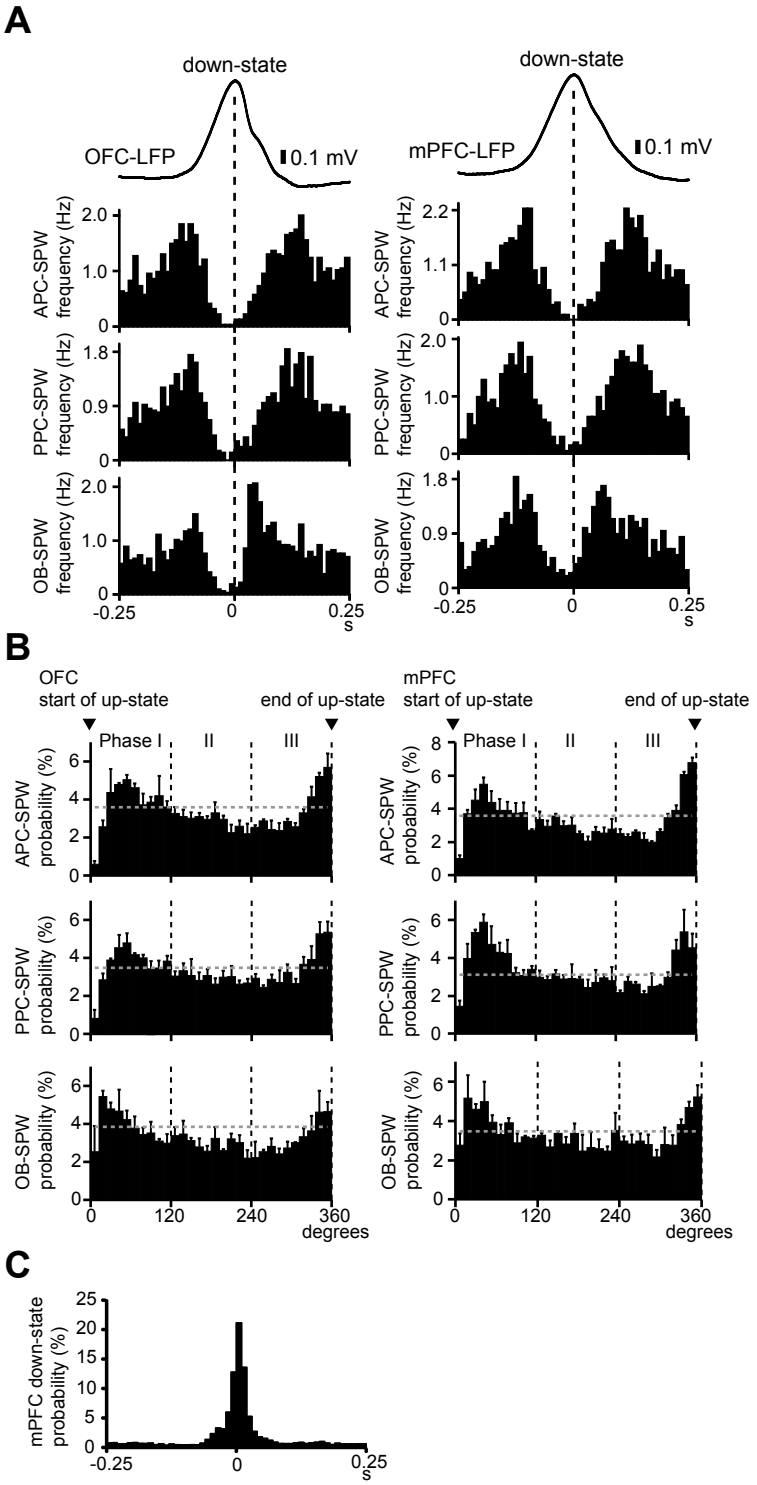
A
down-state
OFC-LFP
0.1 mV
down-state
mPFC-LFP
0.1 mV
APC-SPW frequency (Hz)
PPC-SPW frequency (Hz)
OB-SPW frequency (Hz)
-0.25
0
0.25
s
B
OFC
start of up-state
end of up-state
mPFC
start of up-state
end of up-state
Phase I
II
III
APC-SPW probability (%)
PPC-SPW probability (%)
OB-SPW probability (%)
0
120
240
360
degrees
C
mPFC down-state probability (%)
-0.25
0
0.25
s

Figure 9